Astronomy
&
Astrophysics

# The CARMENES search for exoplanets around M dwarfs

## Variability of the He I line at 10830 Å[*]

B. Fuhrmeister[1], S. Czesla[1], L. Hildebrandt[1], E. Nagel[1,12], J. H. M. M. Schmitt[1], S. V. Jeffers[2], J. A. Caballero[3],
D. Hintz[1], E. N. Johnson[2], P. Schöfer[2], M. Zechmeister[2], A. Reiners[2], I. Ribas[4,5], P. J. Amado[6], A. Quirrenbach[7],
L. Nortmann[2], F. F. Bauer[6], V. J. S. Béjar[8,9], M. Cortés-Contreras[3], S. Dreizler[2], D. Galadí-Enríquez[11],
A. P. Hatzes[12], A. Kaminski[7], M. Kürster[13], M. Lafarga[4,5], and D. Montes[10]

[1] Hamburger Sternwarte, Universität Hamburg, Gojenbergsweg 112, 21029 Hamburg, Germany
    e-mail: bfuhrmeister@hs.uni-hamburg.de
[2] Institut für Astrophysik, Friedrich-Hund-Platz 1, 37077 Göttingen, Germany
[3] Centro de Astrobiología (CSIC-INTA), ESAC, Camino Bajo del Castillo s/n, 28692 Villanueva de la Cañada, Madrid, Spain
[4] Institut de Ciències de l'Espai (CSIC), Campus UAB, c/ de Can Magrans s/n, 08193 Bellaterra, Barcelona, Spain
[5] Institut d'Estudis Espacials de Catalunya, 08034 Barcelona, Spain
[6] Instituto de Astrofísica de Andalucía (CSIC), Glorieta de la Astronomía s/n, 18008 Granada, Spain
[7] Landessternwarte, Zentrum für Astronomie der Universität Heidelberg, Königstuhl 12, 69117 Heidelberg, Germany
[8] Instituto de Astrofísica de Canarias, c/ Vía Láctea s/n, 38205 La Laguna, Tenerife, Spain
[9] Departamento de Astrofísica, Universidad de La Laguna, 38206 Tenerife, Spain
[10] Facultad de Ciencias Físicas, Departamento de Física de la Tierra y Astrofísica; IPARCOS-UCM (Instituto de Física de Partículas
    y del Cosmos de la UCM), Universidad Complutense de Madrid, 28040 Madrid, Spain
[11] Centro Astronómico Hispano-Alemán (MPG-CSIC), Observatorio Astronómico de Calar Alto, Sierra de los Filabres, 04550 Gérgal,
    Almería, Spain
[12] Thüringer Landessternwarte Tautenburg, Sternwarte 5, 07778 Tautenburg, Germany
[13] Max-Planck-Institut für Astronomie, Königstuhl 17, 69117 Heidelberg, Germany

## ABSTRACT

The He I infrared (IR) triplet at 10830 Å is known as an activity indicator in solar-type stars and has become a primary diagnostic in exoplanetary transmission spectroscopy. He I IR lines are a tracer of the stellar extreme-ultraviolet irradiation from the transition region and corona. We study the variability of the He I triplet lines in a spectral time series of 319 M dwarf stars that was obtained with the CARMENES high-resolution optical and near-infrared spectrograph at Calar Alto. We detect He I IR line variability in 18% of our sample stars, all of which show Hα in emission. Therefore, we find detectable He I variability in 78% of the sub-sample of stars with Hα emission. Detectable variability is strongly concentrated in the latest spectral sub-types, where the He I lines during quiescence are typically weak. The fraction of stars with detectable He I variation remains lower than 10% for stars earlier than M3.0 V, while it exceeds 30% for the later spectral sub-types. Flares are accompanied by particularly pronounced line variations, including strongly broadened lines with red and blue asymmetries. However, we also find evidence for enhanced He I absorption, which is potentially associated with increased high-energy irradiation levels at flare onset. Generally, He I and Hα line variations tend to be correlated, with Hα being the most sensitive indicator in terms of pseudo-equivalent width variation. This makes the He I triplet a favourable target for planetary transmission spectroscopy.

**Key words.** stars: activity – stars: chromospheres – stars: late-type

## 1. Introduction

Late-type stars are known to show "activity", which is a term that summarises a zoo of phenomena fuelled by energy from the stellar magnetic field. In particular, M dwarfs frequently exhibit strong activity as evidenced, for example, by coronal X-ray radiation (e.g. Pizzolato et al. 2003; Robrade & Schmitt 2005), prominent chromospheric emission lines (Gizis et al. 2000; Walkowicz & Hawley 2009; Houdebine 2012;

Kowalski et al. 2017), variable temperature-sensitive molecular bands (Schöfer et al. 2019), or high levels of photometric modulation (Rebull et al. 2016; Suárez Mascareño et al. 2016; Díez Alonso et al. 2019).

As a result of new observational possibilities, one chromospheric activity tracer, the He I infrared (IR) triplet at 10830 Å, has recently become a highly promising diagnostic of the outer atmospheres of exoplanets and their dynamics (e.g. Spake et al. 2018; Salz et al. 2018; Nortmann et al. 2018; Allart et al. 2018; Mansfield et al. 2018; Alonso-Floriano et al. 2019). This IR triplet is the only known tracer of planetary mass loss observable from the ground. Planetary transmission spectroscopy is based on the analysis of changes in the profiles and depths of

---

the observed spectral lines. Effects attributable to activity-related temporal variability or an inhomogeneous line profile distribution across the stellar disc, such as those produced by active regions, are major nuisances in the study of exoplanetary atmospheres. Studying the He I transmission signal of HD 189733 b, Salz et al. (2018) estimate that a pseudo-signal introduced by stellar activity of the K-dwarf host star HD 189733 might be responsible for up to 80% of their measured signal. On the other hand, Cauley et al. (2018) used simulations to find that the He I IR line should be less affected by contamination caused by stellar activity than other chromospheric lines. Nevertheless, knowledge of stellar line variability is a crucial ingredient in studies of exoplanetary spectra.

Activity-induced variability occurs on very different timescales. Short-term variability can be caused by transient events such as flares, which are frequently observed on M dwarfs both in photometric light curves (e.g. Walkowicz et al. 2011; Hawley et al. 2014; Yang et al. 2017; Doyle et al. 2018) and spectroscopic observations (Hawley & Pettersen 1991; Fuhrmeister et al. 2008; Schmidt et al. 2012). The flare frequency increases along the M-dwarf sequence with flare duty cycles reaching 3% for late-type M dwarfs (Hilton et al. 2010). On the rotational timescale, ramifications of photospheric spots and chromospheric plages can be observed when they rotate across the visible hemisphere (Barnes et al. 2017; Suárez Mascareño et al. 2018; Newton et al. 2017; Díez Alonso et al. 2019). Finally, activity cycles can impose long-term modulation on the scale of years (Baliunas et al. 1995; Berdyugina & Järvinen 2005; Suárez Mascareño et al. 2016).

To study activity spectroscopically activity-sensitive chromospheric emission lines are used, the best known are the Ca II H & K lines at 3968 and 3934 Å (Baliunas et al. 1995; Wright et al. 2004). Since M dwarfs are rather faint in the blue wavelength range, studies of these lines require a substantial observational effort (Walkowicz & Hawley 2009). Additionally, Ca II IR triplet lines at around 8500 to 8600 Å can be used as variability tracers, although they are not as sensitive as H&K lines (Martin et al. 2017; Jeffers et al. 2018). The same applies to the He I D$_3$ line at 5876 Å and the neighbouring Na I D doublet lines, which can moreover be affected by airglow (Hossain et al. 2014). As a consequence, many activity studies of M dwarfs have focussed on the very sensitive and accessible H$\alpha$ line, which however may not sample the same phenomena as Ca II H & K lines (Walkowicz & Hawley 2009; Jeffers et al. 2018; Schöfer et al. 2019).

Prominent activity-sensitive lines in the near-infrared (NIR) regime are the He I IR triplet lines at (vacuum) wavelengths of 10 832.057, 10 833.217, and 10 833.306 Å. This triplet is formed by transitions between the meta-stable $2^3$S and the $2^3$P levels. The two reddest components dominate the triplet and remain unresolved in the majority of studies, which is why we refer to this complex as the He I IR line for short. While the He I line has long been studied in the Sun (e.g. Vaughan & Zirin 1968; Zirin 1982), it is a relatively new addition in the context of stellar observations (Sanz-Forcada & Dupree 2008; Andretta et al. 2017); these observations have only become feasible after the advent of suitable high-resolution infrared spectrographs. As the meta-stable $2^3$S state of neutral helium has an excitation potential of about 20 eV, it is thought to be populated by photo-ionisation–recombination processes triggered by extreme-ultraviolet (EUV) and X-ray emission from the stellar transition region and corona with wavelengths below the helium ionisation edge at 504 Å (Zirin 1988). This makes the He I line a prominent tracer of the stellar EUV emission, which is typically heavily

affected by interstellar absorption and not directly observable with ground-based instrumentation.

A highly stabilised spectrograph, CARMENES simultaneously covers the optical and near-infrared range, including the He I IR line region, at high resolution (Sect. 2). This has made it a prime instrument to study both planetary and stellar He I lines. In Fuhrmeister et al. (2019a), we present a systematic study of the He I IR line in M dwarfs with a focus on the time-averaged properties of the line. Our study shows that the line is usually a strong feature in early M dwarfs. Yet, its pseudo-equivalent width (pEW) decreases towards later spectral sub-types becoming undetectable around sub-type M5.0 V (see also Sect. 3). We revisit the spectral time series of the 319 stars also considered in Fuhrmeister et al. (2019a) and extend our previous analysis into the time domain; we also examine the variability amplitude of the He I IR line, the relation to other activity indicators, and its behaviour during flares. We intend to interpret this in terms of the reliability of He I IR line detection and analysis of exoplanet atmospheres (Seager & Sasselov 2000).

Our paper is structured as follows: in Sect. 2 we give an overview of the used data and our method for pEW measurements. Subsequently we describe our findings on variability in the He I IR line in Sect. 3, while in Sect. 4 we concentrate on some outstanding examples and the conclusions we draw thereof. In Sect. 5 we point out the implications for exoplanet atmosphere studies analysing the He I IR line. Finally, in Sect. 6, we summarise our findings.

## 2. Observations and measurement method

### 2.1. Used data and their reduction

All spectra used for the present analysis were taken with the CARMENES spectrograph, mounted at the 3.5 m Calar Alto Telescope (Quirrenbach et al. 2016). The CARMENES instrument is a highly stabilised spectrograph covering the wavelength range from 5200 to 9600 Å in the visual channel (VIS) and from 9600 Å to 17 100 Å in the NIR channel. The instrument provides a spectral resolution of ~94 600 in VIS and ~80 400 in NIR. The CARMENES consortium is conducting a 750-night survey, targeting ~350 M dwarfs to find low-mass exoplanets (Alonso-Floriano et al. 2015; Reiners et al. 2018). To date, CARMENES has obtained more than 16 000 high-resolution visible and NIR spectra. Since the cadence of the spectra is optimised for the planet search, as a rule no continuous time series are obtained and the typical observing frequency is at maximum once per night.

The spectra of the monitored 319 stars were reduced using the CARMENES reduction pipeline (Zechmeister et al. 2014). Subsequently, they were corrected for barycentric and other radial velocity motions, as well as for secular acceleration and telluric absorption (Nagel et al. 2019) using the `molecfit` package[1]. The He I IR line region is contaminated with OH airglow lines. The four relevant lines belong to two so-called Λ-doublets at wavelengths of 10 834.241 and 10 834.338 Å and 10 832.412 and 10 832.103 Å (Phillips et al. 2004; Oliva et al. 2015). The redder doublet remains unresolved and is the stronger one. All lines correspond to transitions between levels with vibrational quantum numbers of five and two and the same rotational quantum number, which suggests a relation between their intensities. We

---

[1] https://www.eso.org/sci/software/pipelines/skytools/molecfit

**Table 1.** Parameters of the pEW calculation.

| | Line | Full width | Reference band 1 | Reference band 2 |
|---|---|---|---|---|
| | [Å] | [Å] | [Å] | [Å] |
| He I IR | 10 833.26 | 1.6 | 10 820.0–10 822.5 | 10 851.0–10 853.0 |
| H$\alpha$ | 6564.62 | 1.6 | 6537.43–6547.92 | 6577.88–6586.37 |
| Ca II IRT$_1$ | 8500.33 | 0.5 | 8476.33–8486.33 | 8552.35–8554.35 |
| He I D$_3$ | 5877.24 | 1.0 | 5870.00–5874.00 | 5910.0–5914.0 |

used around 1600 sky-fibre spectra obtained by CARMENES to verify this hypothesis and determined the intensity ratio between the doublets by fitting Gaussian components to the OH sky spectra. As the redder doublet tends to be prominent in the science spectrum, we used it to constrain the normalisation of the thus determined OH model with fixed intensity ratios and subtracted it from the science spectrum. This procedure led to a substantial reduction of the telluric line contamination. Naturally, however, some spectra remain affected by varying degrees of correction artefacts.

### 2.2. Equivalent width measurement

We measured the pEW of the He I IR line, the H$\alpha$ line, the bluest component of the Ca II infrared triplet lines (Ca II IRT$_1$ line), and the He I D$_3$ line. For the He I IR line we treated the blended two reddest components as one single line at 10 833.26 Å. The precise integration and reference bands are given in Table 1. Thus, a time series of pEW measurements was obtained for each star. From these pEW time series, we calculated the mean pEW and the median average deviation about the median (MAD), which is a robust estimator of the scatter (Hampel 1974; Rousseeuw & Croux 1993; Czesla et al. 2018). For a Gaussian distribution, the MAD multiplied by 1.4826 is an estimator of the standard deviation. We decided not to use the mean average deviation of the mean because it is more severely influenced by outliers that are mainly caused by artefacts such as cosmic rays and leftovers from the telluric correction in the case of the He I IR line. The error of the pEW depends strongly on the signal-to-noise ratio of the spectra and is, therefore, much lower for a bright early M dwarf than for a fainter mid-type M dwarf because the exposure times never exceed 1800 s. Moreover, the pEW(He I) changes if there are artefacts included in the integration interval.

Finally, we quantified the degree of correlation between the pEW time series of the He I IR line and the H$\alpha$, He I D$_3$, and Ca II IRT$_1$ lines by computing Pearson's correlation coefficient $r$ and their $p$-values. For comparison, we also computed Pearson's correlation coefficient for the pEW time series of the H$\alpha$ and Ca II IRT$_1$ lines. In Table 2, we list the values for all stars identified by their CARMENES identification (Karmn); the full tables are available at CDS.

### 2.3. Error analysis

To investigate the uncertainty in the pEW measurements and the resulting MAD values, we looked at the lowly active M1.5 V star J00051+457 (GJ 2). Since GJ 2 shows a typical number, strength, and position of artefacts, we used it as a reference. The H$\alpha$ line spectra of GJ 2 display variability at a low level (Fig. 1) and there is a correlation between the pEW(H$\alpha$) and pEW(Ca II IRT$_1$) with a value of 0.69 for Pearson's correlation coefficient ($p = 5.5 \times 10^{-6}$). However, there is no correlation

with the pEWs of the He I IR line because it is not sensitive enough, as we discuss below. We deem the He I IR line of GJ 2 intrinsically stable.

The statistical uncertainty of pEW(He I IR) is small as can be seen in Fig. 1, where the error bars are smaller than the used symbols. Indeed the relative error is about one percent; while for pEW(H$\alpha$) it is about six percent. If this were the only source of variation, this should be reflected by the standard deviation of the values in the time series. However, the latter value is about four times higher than the statistical uncertainty, demonstrating that the variation of the pEW measurements is dominated by other effects caused by, for example telluric correction, cosmics, instrumental effects, or normalisation problems.

To obtain an error estimate on the MAD, we used the bootstrap method. In particular, we generated bootstrap samples by randomly selecting pEW measurements (with replacement) from the time series and computed the associated MAD. From the thus obtained distribution, we computed the standard deviation of the MAD, which amounts to about 20% of its original value as well for MAD(He I IR) as for MAD(H$\alpha$). We consider this a lower limit for the achievable precision of the MAD estimate. For stars with fewer observations, the uncertainty on the MAD scales approximately inversely proportional to the square root of the number of data points, reaching around $0.5 \times$ MAD for stars with less than ten spectra. Although the details depend on the individual case, we conclude that an uncertainty estimate of $0.2 \times$ MAD is applicable to the majority of our stars. For the latest sub-type stars with high levels of statistical noise in their spectra and for some stars with much stronger artefacts this estimate may be too low.

## 3. General He I IR line variability properties

In this section we briefly summarise our findings about the time-average properties of the He I IR line from Fuhrmeister et al. (2019a), which represent the quiescent state of the star. In the latter paper we find that the observed strength of the line depends on the spectral type or effective temperature: in early-type M dwarfs it manifests itself ubiquitously as a strong absorption line with pEW(He I IR) up to 300 mÅ, which declines to later spectral sub-types and becomes undetectable with the methods used by Fuhrmeister et al. (2019a) at about M5 (and pEW(He I IR) < 50 mÅ for the stars with the best signal-to-noise ratio (S/N)). We attribute the few cases in which the line is found in emission in the average spectrum to flaring activity strong or frequent enough to affect the average spectrum.

### 3.1. He I IR line variability

For an automatic detection of variability we looked at the scatter in the data that we measured with the MAD. In Fig. 2 we compare the MADs of the pEW measurements of the H$\alpha$ and He I IR lines. The star with the largest MAD(H$\alpha$) is J05084-210 (2M J05082729-2101444) and the star with the highest MAD(He I IR) is J01352-072 (Barta 161 12); both are young stars (see Table 3) and are discussed in Sect. 4 in more detail. As seen in Fig. 2, the pEW scatter in the H$\alpha$ line is about 30 times larger than that in the He I IR line, while the integration band widths of 1.6 Å are identical (Table 1). Therefore, the H$\alpha$ line is considerably more variable in each time series and, as a consequence, it also shows larger variations within our sample of stars and is thus also a more sensitive activity indicator than the He I IR line. Figure 2 shows that most stars for which the He I IR line could be detected in the average spectra by Fuhrmeister et al.

**Table 2.** Measured mean pEWs, MADs, and correlation coefficients of the considered lines.

| Karmn | Corr He I IR- Hα | p-val | Corr He I IR- He ID₃ | p-val | Corr He I IR- Ca II IRT₁ | p-val | Corr Hα- Ca II IRT₁ | p-val | Mean pEW (He I IR) [Å] | Mean pEW (Hα) [Å] | Mean pEW (He ID₃) [Å] | Mean pEW (Ca II IRT₁) [Å] | MAD (He I IR) [Å] | MAD (Hα) [Å] | MAD (He ID₃) [Å] | MAD (Ca II IRT₁) [Å] |
|---|---|---|---|---|---|---|---|---|---|---|---|---|---|---|---|---|
| J00051+457 | 0.215 | 0.148 | 0.291 | 0.047 | −0.030 | 0.843 | 0.609 | 0.000 | 0.225 | 0.343 | −0.026 | 0.748 | 0.004 | 0.019 | 0.003 | 0.006 |
| J00067−075 | −0.029 | 0.813 | −0.111 | 0.362 | 0.290 | 0.015 | 0.427 | 0.000 | 0.017 | −0.071 | 0.053 | 0.402 | 0.004 | 0.050 | 0.024 | 0.009 |
| J00162+198E | 0.269 | 0.484 | −0.350 | 0.356 | 0.342 | 0.368 | 0.878 | 0.002 | 0.065 | 0.094 | −0.016 | 0.553 | 0.014 | 0.011 | 0.010 | 0.007 |
| J00183+440 | 0.443 | 0.000 | −0.217 | 0.003 | 0.037 | 0.615 | 0.136 | 0.063 | 0.105 | 0.311 | −0.003 | 0.793 | 0.005 | 0.007 | 0.004 | 0.002 |
| J00184+440 | 0.560 | 0.000 | −0.583 | 0.000 | 0.862 | 0.000 | 0.651 | 0.000 | 0.025 | 0.154 | 0.049 | 0.765 | 0.005 | 0.014 | 0.005 | 0.002 |
| J00286−066 | −0.673 | 0.002 | 0.095 | 0.708 | −0.595 | 0.009 | 0.568 | 0.014 | 0.075 | 0.134 | −0.021 | 0.536 | 0.005 | 0.015 | 0.011 | 0.004 |
| J00389+306 | 0.149 | 0.568 | 0.006 | 0.982 | −0.345 | 0.175 | 0.387 | 0.125 | 0.139 | 0.281 | −0.026 | 0.743 | 0.006 | 0.015 | 0.007 | 0.007 |
| J00570+450 | −0.309 | 0.456 | −0.162 | 0.702 | −0.575 | 0.136 | 0.752 | 0.031 | 0.118 | 0.130 | −0.028 | 0.671 | 0.005 | 0.034 | 0.005 | 0.004 |
| J01013+613 | −0.071 | 0.856 | −0.232 | 0.548 | −0.151 | 0.698 | 0.983 | 0.000 | 0.133 | 0.203 | −0.026 | 0.737 | 0.005 | 0.047 | 0.003 | 0.003 |
| J01019+541 | 0.262 | 0.294 | 0.295 | 0.235 | 0.301 | 0.225 | 0.971 | 0.000 | 0.136 | −4.462 | −0.813 | 0.183 | 0.038 | 0.447 | 0.072 | 0.024 |

. . .

**Notes.** The full table is provided at CDS. We show the first 10 rows as a guideline.

(2019a) do not show variability, while there are a number of stars for which the line could not be detected in the average spectra, but reveals itself now by variability. This latter case is discussed below.

Moreover, Fig. 2 shows that there are two groups of stars: an inactive group at the bottom left and an active group with higher variability at the top right. The majority of our sample stars belong to the inactive group and show only low levels of variability in the pEW(Hα) as measured by MAD(Hα) < 0.1 Å. These sample stars nevertheless may display the full range of observed MAD(He I IR). In particular, there are five stars with MAD(He I IR) greater than 0.038 Å and low MAD(Hα). Visual inspection shows that many spectra of these stars are subject to artefacts of cosmic rays and airglow in the spectral range of the He I IR line, thereby leading to a large spurious MAD(He I IR) without physical reason but caused by long exposure times because all five are rather faint stars. In contrast, all 11 stars with MAD(Hα) > 0.75 Å are also found variable in the He I IR line. Before we define our variability criterion in the next section, we want first to present an example of an inactive and an active star.

To give an example for line variability in inactive stars, we refer again to Fig. 1 in which we show all available He I IR and Hα line spectra of the weakly active star GJ 2. The correlation behaviour of the lines was already discussed in Sect. 2.2. The spectra show a prominent He I IR line along with a Si I line at 10 830.057 Å and a Na I line at 10 837.814 Å. All other spectral features in the shown wavelength range remain unidentified; see a discussion in Fuhrmeister et al. (2019a) and compare to Andreasen et al. (2016) and Marfil et al. (2020). Figure 1 also shows that telluric lines are a minor problem around the Hα line. As can be seen from Table 2, the MAD(Hα) and MAD(He I) are 0.019 and 0.004 Å, respectively, and therefore well within the cloud at the lower left seen in Fig. 2, which should represent stars with low levels of activity.

In contrast the M3.0 star J03473-019 (G 080-021) provides an example of a more active star. The nine available CARMENES spectra, as can be seen in Fig. 3, show that the Hα line is always in emission with obvious variability. The He I IR line also displays clear variability going from absorption into emission. As a consequence, the line is almost absent in the average spectrum, which is consistent with our previous non-detection

in Fuhrmeister et al. (2019a). The pEW(He I IR) is correlated with all of pEW(Hα); pEW(He ID₃),which is in emission; and pEW(Ca II IRT₁). Also, pEW(Hα) and pEW(Ca II IRT₁) are correlated. All correlation coefficients are higher than 0.94 with $p < 10^{-4}$. Concerning the variability as measured by the MAD(Hα) and MAD(He I) of 0.273 and 0.024 Å, respectively, the star is located in the top part of Fig. 2.

### 3.2. Conservative He I variable sample

Visual inspection proves that for some stars the identification of variability in the He I IR line remains ambiguous, mostly because of the artefacts found in the line region. Therefore, we proceed to identify the stars showing the most reliably physical variation in the He I IR line. To this end, we demand that both the Hα and He I IR lines show significant scatter in their pEW measurements. We define the conservative He I variability sample (conservative sample for short) to comprise all stars with MAD(Hα) > 0.08 and MAD(He I IR) > 0.01 Å. This roughly corresponds to the borderlines between the clouds of the least active stars at the bottom left and the most active stars at the top right in Fig. 2. A total of 56 stars (18% of the sample) show variability on this level. This conservative sample is very similar to the stars we found by visual inspection of their spectra to be variable, therefore emphasising the robustness of the method. Moreover, we used the visual inspection to fine-tune the thresholds in MAD(Hα) and MAD(He I IR).

All stars in the conservative sample show Hα in emission, which we define by pEW(Hα) < −0.6 Å following Fuhrmeister et al. (2019a). In fact, only such stars match the MAD(Hα) > 0.08 criterion. About 80% of the Hα emitters are included in the conservative sample as well as approximately the same fraction of the fast rotators ($v \sin i > 25$ km s$^{-1}$). On the other hand, for most stars in which we find the He I IR line to be variable, the line was not found in the averaged spectra in our previous study and the mean pEW(He I) differs only marginally from zero. This indicates that either the line varies from absorption to emission in these stars and, therefore, is hardly visible in the average spectrum, or the line is not present in the spectra during quiescence and only evolves into emission during flares. For the first case, we already showed an example in Fig. 3, while for the second case more examples are presented in Sect. 4.
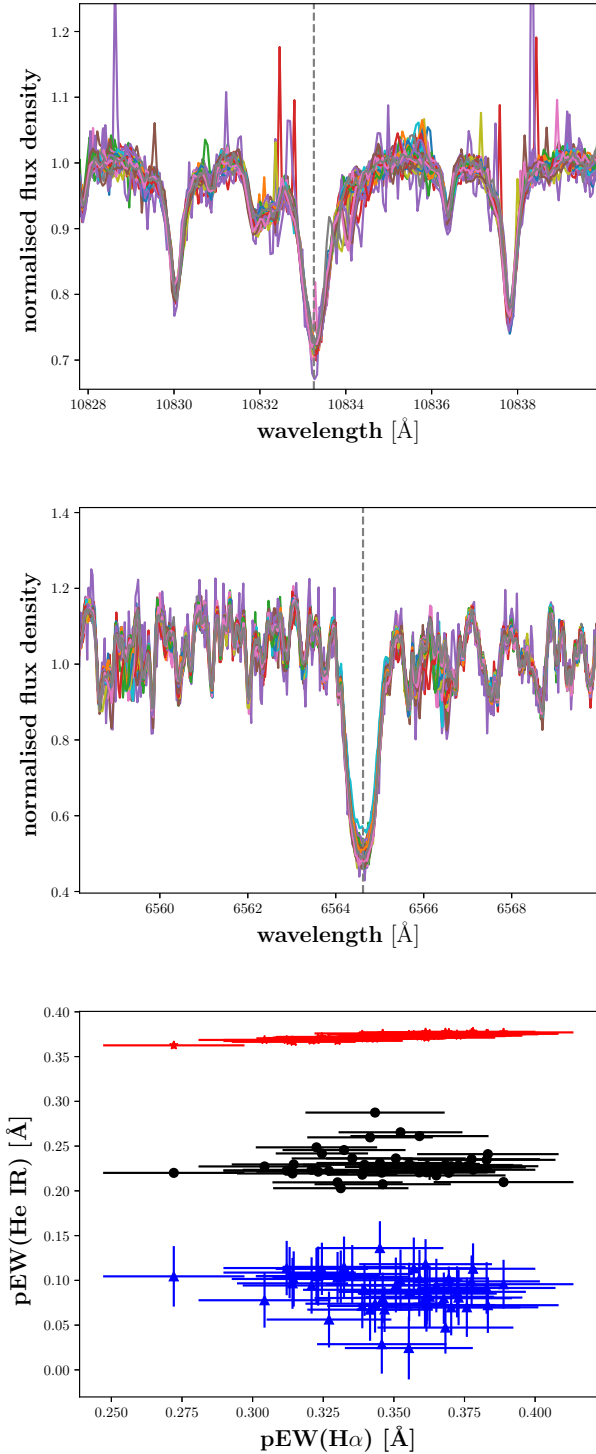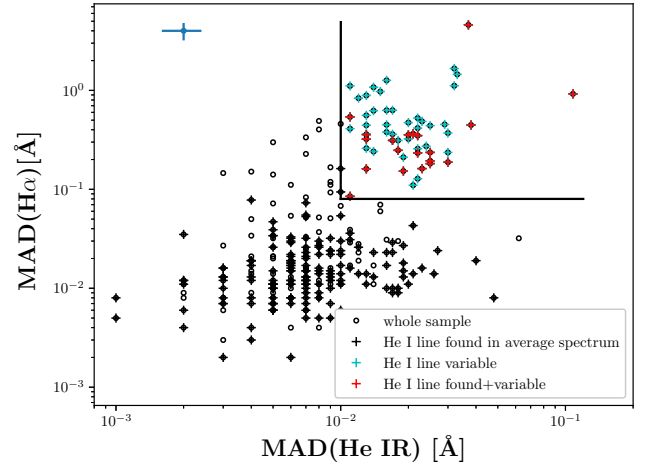
**Fig. 2.** Median average deviation (Hα) as a function of MAD(He I IR) for the sample stars (black open circles). The black crosses indicate stars for which the He I IR line was detected in the averaged spectra by Fuhrmeister et al. (2019a). The cyan crosses indicate stars where the line could not be found in the average spectrum but is detectable by He I IR line variability, and the red crosses denote stars with both properties. The error bars shown at the top left corner illustrate the 20% systematic error estimated as described in Sect. 2.2. The black vertical and horizontal lines denote the thresholds for our conservative variable He IIR line sample as defined in Sect. 3.2.

two M2.0 dwarfs J09425+700 (GJ 360) and J11201-104 (LP 733-099). These two latter stars are significantly variable in Hα, but visual inspection shows that the He I IR line is again subject to artefacts. This lack of He I IR line variability in early M dwarfs is connected to the general inactivity of these stars. Although they display a chromosphere, its contribution to the spectrum is not strong and variable enough (or both) to be significant in this type of analysis. At spectral type M3.0, a steep increase in the number and fraction of variable stars occurs, which reaches a peak at M4.0 and then decreases again towards M6–6.5. We show this behaviour in Fig. 4, together with the behaviour of the ratio of MAD(He I) and MAD(Hα). Overall, the pEW variation as measured by the MAD is about an order of magnitude larger in Hα than in the He I IR line. The distribution appears to show a trend to lower ratios for later-type stars indicating that the variability in the He I IR line declines relative to that in Hα. This may correspond to the decline of the line strength in He I IR found in our previous study. Nevertheless, we find that out of the 23 M5.0 dwarfs, 13 match the criterion of the conservative sample, although Fuhrmeister et al. (2019a) was able to find the He I IR line in the average stellar spectra for only one of these stars. Among the 22 stars with later spectral types, we found variations in only two owing to the increasing noise in the spectra.

### 3.3. Correlation between pEW values for different chromospheric lines

For most of the 56 stars in the conservative sample, pEW(Hα) is well correlated to pEW(Ca II IRT$_1$) with a mean Pearson's correlation coefficient of $r = 0.87$. Furthermore, 30 stars also show a correlation between pEW(Hα) and pEW(He I) with $r > 0.6$ and a $p$-value below 0.05 (which we regard as the highest $p$-value for a significant correlation). Although many of these stars show prominent signs of flaring in at least some of their spectra, there are also a few spectral time series without clear flare signatures (see Fig. 3).

**Fig. 1.** All available spectra of the M1.5 V star GJ 2. *Top*: region around the He I IR line. Some artefacts of airglow and cosmics manifest themselves as emission spikes. *Middle*: region around Hα. Minor telluric contamination at about 6559–6560 and 6566–6567 Å is evident. The dashed vertical lines indicate the central wavelength of the He I IR and Hα lines, respectively. *Bottom*: correlation for different chromospheric lines to pEW(Hα). Black denotes pEW(He I IR), blue denotes pEW(He I D$_3$) scaled by −4, and red denotes pEW(Ca II IRT$_1$) scaled by 0.5.

The earliest star in the conservative sample is the M1.5 dwarf J15218+209 (OT Ser), which is known to be young (Shkolnik et al. 2009) and active (Shulyak et al. 2019), followed by the

**Table 3.** Stellar parameters of the discussed variable stars.

| Karmn | Name | Spectral type | $v \sin i$ [km s$^{-1}$] | $P_{\rm rot}$ [d] | Moving group |
|---|---|---|---|---|---|
| J01352−072 | Barta 161 12 | M4.0 V (Ria06) | 59.8 ± 6.9 (Rein18) | 0.7 (Kira12) | β Pic (Malo14) ... |
| J02519+224 | RBS 365 | M4.0 V (Ria06) | 27.2 ± 2.7 (Rein18) | 0.86 (DA19) | LA (CC20) |
| J05084−210 | 2MASS J05082729−2101444 | M5.0 V (Ria06) | 25.2 ± 2.5 (Rein18) | ... | β Pic (Malo14) |
| J06318+414 | LP 205−044 | M5.0 V (PMSU) | 58.4 ± 26.1 (Rein18) | 0.30 (DA19) | LA (CC20) |
| J07472+503 | 2MASS J07471385+5020386 | M4.0 V (Lep13) | 10.1 ± 1.5 (Rein18) | 1.32 ± 0.01 (DA19) | UMa (CC20) |
| J11474+667 | 1RXS J114728.8+664405 | M5.0 V (AF15) | 2.7 ± 1.5 (Rein18) | ... | Cas (CC20) |
| J22231−176 | LP 820−012 | M4.5 V (PMSU) | <2 (Rein18) | ... | ... |
| J22468+443 | EV Lac | M3.5 V (PMSU) | 5.9 ± 0.1 (Fou18) | 4.38 ± 0.03 (DA19) | UMa (CC20) |
| J22518+317 | GT Peg | M3.0 V (PMSU) | 13.2 ± 0.9 (Fou18) | 1.63 ± 0.01 (DA19) | ... |

**References.** AF15: Alonso-Floriano et al. (2015); CC20: Cortes-Contreras et al. (in prep.); DA19: Díez Alonso et al. (2019); Fou18: Fouqué et al. (2018); Kira12: Kiraga (2012); Lep13: Lépine et al. (2013); Malo14: Malo et al. (2014); PMSU: Reid et al. (1995); Rein18: Reiners et al. (2018); Ria06: Riaz et al. (2006).

To illustrate the correlations better we show the time series of six stars out of the 19 M4.0 dwarfs in Fig. 5. These stars were selected for their representative number of spectra and a broad coverage in pEW(Ca II IRT$_1$) and pEW(He I). Besides a few stars with low or negative correlation values that have non-significant $p$-values, all the M4.0 dwarfs show similar slopes of their linear approximations. Many stars have one or two outliers in their pEW(He I). For example, for J02519+224 (RBS 365) the Pearson's correlation coefficient is 0.46, and amounts to 0.63 without the outlier in pEW(He I), which is caused by a flare. The similarity in the slopes is not necessarily expected, since our variability criterion is not tied to correlation but only to variation. Since Hα is thought for M dwarfs to first deepen with increasing activity levels before going into emission (Cram & Mullan 1979), it is possible to also naively expect negative correlation. For the Sun and solar-like stars the correlation coefficient between Hα and the Ca II H and K lines for example may vary from −1 to 1 for different stars. This was explained by Meunier & Delfosse (2009) mainly by different filling factors and contrasts between plages and filaments. In our sample no significant negative correlation was found. Moreover, all 15 stars among the conservative sample with $r < 0.5$ for the correlation between pEW(Hα) and pEW(He I) turned out to be caused by outliers either because of low S/Ns, airglow artefacts, or even flaring (in case the lines do not react in the same fashion to the flare). Discarding these outliers leads to significant correlation of the time series. Therefore, we conclude, that variability in the He I IR line always comes with a positive correlation to pEW(Hα).

### 3.4. Rotational variability

Besides the strong variability detected by our method there may be much lower amplitude variations in the sample that are nevertheless correlated, if they are caused for example by the plage rotating with the star. Rotational modulation is a source of variability in chromospheric indicators and provides one possibility to measure rotation periods (Mittag et al. 2017; Fuhrmeister et al. 2019b). Unfortunately, we have fewer than 30 spectra for most of the stars showing a high correlation between pEW(Hα) and pEW(He I), so that a period search is not promising. The low number of spectra for these stars is due to the exoplanet search goal of the survey: active stars were observed a few times and then discarded from the survey after finding that their activity causes radial velocity jitter (Tal-Or et al. 2018).

There are 20 stars showing values larger than 0.7 for Pearson's correlation coefficient between pEW(Hα) and pEW(He I IR) (irrespective of the $p$-value), which are not included in the conservative sample; these stars may exhibit a low level variation that is not detected by our method. However, the majority of these stars suffer again from artefacts or a low number of spectra. We only consider the variation real for three stars: the M5.0 V star J06318+414 (LP 205-044), the M1.0 V star J10251-102 (BD-09 3070), and the M3.0 V star J19084+322 (G 207-019); the latter two have Hα in absorption. However, LP 205-044, which is discussed later among the exceptional examples in Sect. 4, shows Hα in emission and is a fast rotator. Nevertheless, it remains unclear whether the low level variation of these three stars is caused by rotational modulation.

For a further search for rotational modulation we also revisit the cases of J13536+776 (NLTT 35712) and J01026+623 (BD+61 195) to follow up previous reports on rotational modulation in their chromospheric lines. For the M4.0 V star NLTT 35712, Dupree et al. (2018) report He I IR line variation that is consistent with rotational modulation with the known period of 1.231 d (Newton et al. 2016). The star is included in our conservative sample. It shows a high value of 0.77 for Pearson's correlation coefficient between pEW(He I IR) and pEW(Hα), but a rather large $p$-value of 0.08. Looking at the He I IR line spectra reveals that one spectrum shows an artefact and another spectrum was taken during a flare as evidenced by a blue asymmetry in Hα (Fuhrmeister et al. 2018). The seven available spectra were taken between April 2016 and January 2018 each at least about a month apart. In a phase folded time series pEW(Hα) and pEW(He I) do not show a conclusive pattern. This inconclusiveness together with the high amplitude of changes in Hα outside flares seems to indicate that a possible variation with the rotation period is at least veiled if not dominated by intrinsic variability in these lines on the timescales covered in this study.

As a further check for the sensitivity of the He I IR line to rotational modulation, we examine the M1.5 V star BD+61 195, whose period is known to be 18.4 d (Suárez Mascareño et al. 2018, obtained from spectroscopic lines) to 19.9 d (Díez Alonso et al. 2019, obtained photometrically). This star also represents the most benevolent case in our own previous period search based on CARMENES activity indices (Fuhrmeister et al. 2019b), where we recovered the rotation period in the pEW(Hα) and pEW(Ca II IRT$_1$) using a generalised
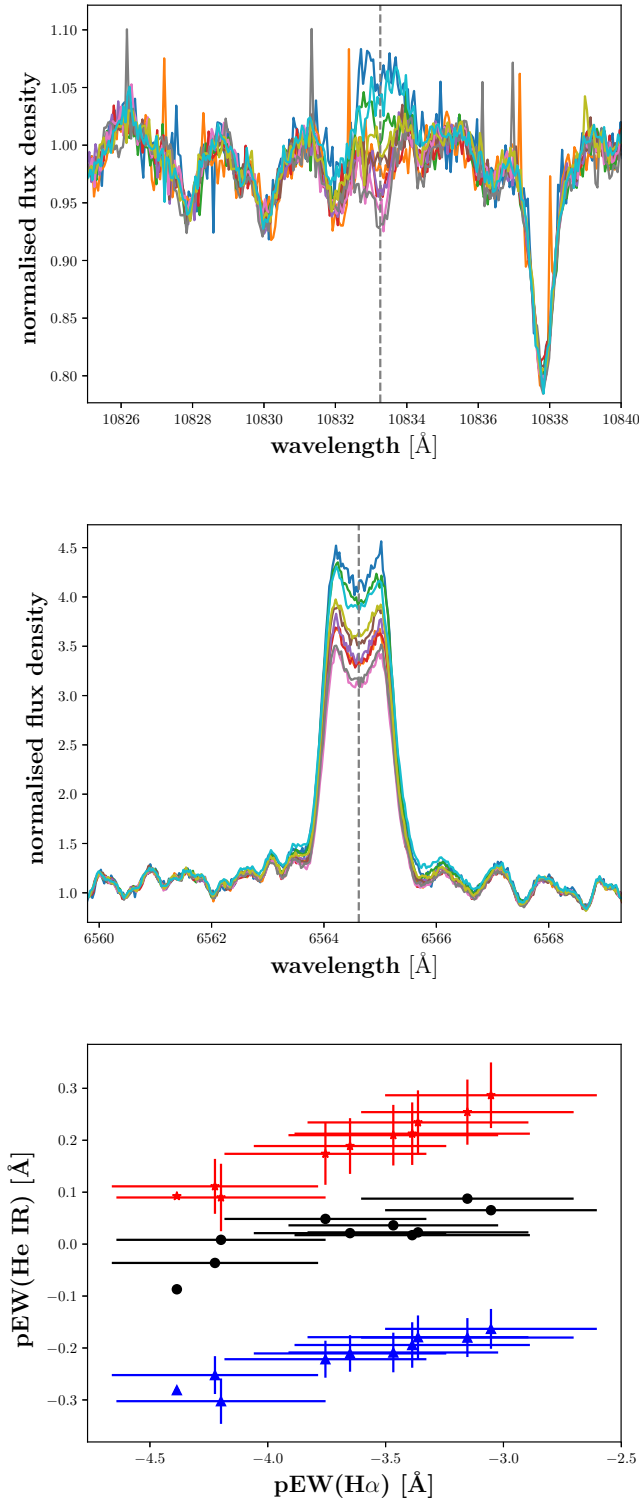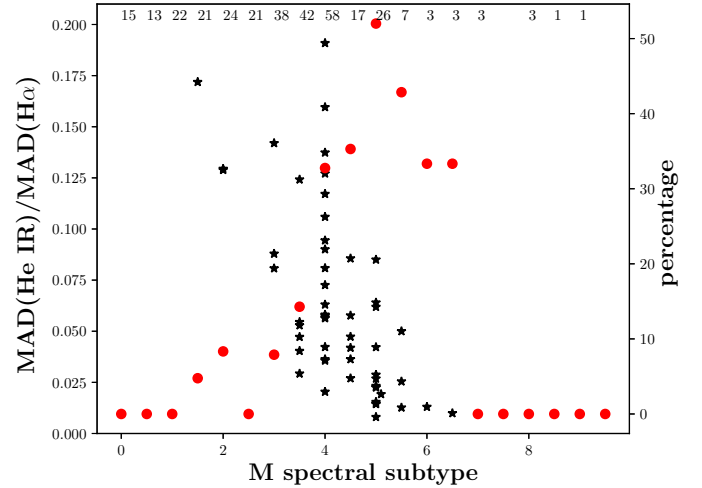
**Fig. 4.** Median average deviation (He I)/MAD(Hα) as a function of spectral sub-type (black asterisks). The dots for the two M2.0 stars lie on top of each other. The red dots correspond to the right axis where we give the percentage of stars found to be variable. The total number of stars for each bin are given at the top of the panel.
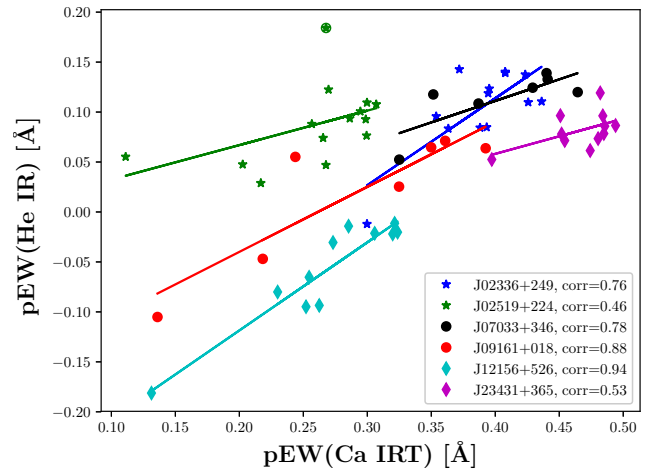


**Fig. 5.** Pseudo-equivalent width(He I) as a function of pEW(Ca II IRT$_1$) for six representative M4.0 stars. Measurements are designated by the symbols, while linear fits to the measurements are given by the solid lines. The CARMENES identification numbers of the stars are given in the legend together with the respective Pearson's correlation coefficient. The outlier caused by a flare for J02519+224/RBS 365 is denoted with an additional circle.



**Fig. 3.** All available spectra of the star G 080-021. *Top*: region around the He I IR line. *Middle*: region around Hα. The dashed vertical lines indicate the central wavelength for the He I IR and the Hα lines, respectively. *Bottom*: correlations for different chromospheric lines to pEW(Hα); black denote pEW(He I IR), red pEW(He I D$_3$) scaled by 0.5, and blue pEW(Ca II IRT$_1$).

Lomb-Scargle periodogram as implemented in PyAstronomy (Zechmeister & Kürster 2009; Czesla et al. 2019) with relative ease. In contrast, no significant period can be established for the pEW(He I IR) time series. We consider this a likely consequence

of the inferior sensitivity of the He I IR line compared to the other indicators.

## 4. Individual examples of variability

### 4.1. Classification of the examples

Since not much is known about the behaviour of the He I IR line in M dwarfs during flaring activity, in this section we present some examples of exceptional line profiles. These examples were selected by visual inspection and the list is not complete with respect to any definitive criterion. Nevertheless, we tried to cover a broad variety of different line profiles, which seem to be typical reactions to different flare phases. Since we only have snapshots, flare identification is not always certain. Therefore, we restricted our examples to spectra for which we identify flaring

**Table 4.** Julian date of major flares for the stars from Table 3.

| Karmn | JD of flare −2450000 [d] | Colour in Fig. | Reference number |
|-------|--------------------------|----------------|------------------|
| RBS 365 | 7693.50903 | Blue | 1 |
| | 7985.61434 | Orange | 2 |
| LP 205-044 | 7823.44073 | Blue | 1 |
| | 8057.63874 | Orange | 2 |
| J07472+503 | 8005.66491 | Blue | 1 |
| | 8031.64099 | Orange | 2 |
| | 8081.56145 | Cyan | 3 |
| J11474+667 | 7762.54635 | Blue | 1 |
| EV Lac | 7632.62893 | Blue | 1 |
| | 7633.46711 | Orange | 2 |
| | 7650.53689 | Green | 3 |
| | 7968.42107 | Red | 4 |
| | 7999.35888 | Purple | 5 |
| | 8032.42971 | Brown | 6 |
| GT Peg | 7762.2768 | Blue | 1 |

activity by line broadening in H$\alpha$. Flares with either symmetric or asymmetric broadening in the H$\alpha$ line almost always show an extraordinary reaction in the He I IR line while flares that manifest themselves only in an amplitude enhancement in H$\alpha$ typically show minor reactions in the He I IR line.

In the case of asymmetric H$\alpha$ line broadening, the asymmetry helps to determine the flare phase. In particular, blue asymmetries are thought to be caused by chromospheric evaporation associated with flare onset and red asymmetries are thought to be caused by coronal rain occurring during the decay phase (Fuhrmeister et al. 2018). Symmetric broadening may be attributable to Stark broadening, turbulence, or an integration effect. Our typical exposure times of 15 min are long compared to the flare timescale so that both signatures of chromospheric evaporation and back-falling material may be caught in the same spectrum. Turbulent broadening may also be responsible for the broadening in asymmetric cases, when the moving material is additionally turbulent.

We sort our examples by the type of broadening observed in H$\alpha$ and thereafter present two exceptional stars, J01352-072 (Barta 161 12) and J06318+414 (LP 205-044), which are most puzzling. In Table 3, we give the spectral type, $v \sin i$, the rotation period, and the moving group the stars belong to (if applicable) for all stars for which we show spectra in this section. For better reference we identify all major flares shown by the Julian date of their occurrence in Table 4.

### 4.2. Blue asymmetries in H$\alpha$

As examples of stars with prominent H$\alpha$ blue asymmetries, we show the spectra of J02519+224 (RBS 365) and J07472+503 (2MASS J07471385+5020386) in Figs. 6 and 7. In RBS 365, the core of the H$\alpha$ line taken in flare spectrum no. 1 shows an average amplitude, accompanied by a strong blue wing enhancement, extending to velocities of about $-450$ km s$^{-1}$ with a peak at $-86$ km s$^{-1}$. This is the only case in which we found signatures of material close to the escape velocity of the star, which is about 500 km s$^{-1}$ for mid- to early-type M dwarfs. We speculate that this integration mainly covers the quiescent state and ends right after flare onset; this can explain the presence of evaporating material without associated core enhancement because there is already heated material but not enough to show up against

the strong average H$\alpha$ core emission. The associated He I IR line profile in RBS 365 is deeper than the quiescent line profile. This is consistent with elevated EUV irradiation at flare onset, which causes stronger He I IR line absorption. The He I D$_3$ line shows no notable change. This is in contrast to the other spectra of this star, where a higher amplitude in H$\alpha$ is seen in combination with some fill-in of the He I IR line and additional emission in the He I D$_3$ line; we show the spectrum no. 2 in Fig. 6 as an example.

One more intriguing example of a flare onset was observed in J07472+503 (2MASS J07471385+5020386), whose spectra are shown in Fig. 7. The H$\alpha$ spectrum of spectrum no. 3 shows a prominent blue asymmetry. Again this coincides with a deepening of the He I IR line that is likely attributable to increased EUV surface illumination, but this line also shows a blue emission wing. The H$\alpha$ and He I IR line wings both extend to velocities of about $-200$ km s$^{-1}$ and peak around $-65$ km s$^{-1}$. Additionally, we noticed a weak blue wing in the He I D$_3$ line. This implies that the densities in the moving material are high enough to drive the line into emission via collisions. The flare spectrum no. 1 in Fig. 7 shows H$\alpha$ core enhancement without wing emission and also seems to cover a flare. The response of the He I IR line is a moderate fill-in. Curiously, the largest pEW(He I IR) is found for the spectrum no. 2, where even an enhancement in the bluest and weakest component of the He I IR triplet at about 10 832 Å can be distinguished. The corresponding H$\alpha$ line profile looks completely innocuous, showing, if anything, a marginal blue wing. We speculate that the He I IR line reacts to an enhanced EUV radiation level even before H$\alpha$ shows a significant response. This is especially important for exoplanet studies of the He I IR line, since it indicates that the reaction of the stellar He I IR line may precede that of H$\alpha$ in flares.

Although two more stars (J06574+740 (2MASS J06572616+7405265) and J06000+027 (G 099-049)) in the sample show a deepening of the He I IR line with no significant change seen in H$\alpha$, also the opposite can be found viz. a significant blue asymmetry in H$\alpha$ with no deepening of the He I IR line. This is seen for example for the star J05084-210 (2MASS J05082729-2101444). The corresponding flares possibly show lower EUV emission levels during onset or the He I IR line response cannot be observed, for example for a flare at or beyond the limb. Another rarely occurring case seems to be the connection between the deepening in the He I IR line and a red asymmetry in H$\alpha$. We could identify only a single spectrum (belonging to J22468+443, hereafter EV Lac) showing a deepening in the He I IR line along with a minor H$\alpha$ red asymmetry.

### 4.3. Red asymmetries in H$\alpha$

We identified a number of spectra showing red H$\alpha$ asymmetries presumably caused by coronal rain in the later stages of flares (Fuhrmeister et al. 2018). Red H$\alpha$ asymmetries seem to be typically accompanied by emission in the He I IR line. This indicates that the flaring material is dense enough to let collisions drive the He I IR line into emission.

As an example with emission in the main He I IR line component but absorption in the wing, in Fig. 8 we show 2 out of 11 spectra of J22518+317 (GT Peg). One spectrum demonstrates the typical quiescent chromospheric emission lines; the other shows a flare spectrum with an H$\alpha$ red asymmetry. In the flaring spectrum, the He I IR line shows a prominent and slightly blue-shifted emission peak and a shallow, broad absorption feature on the red side of the line. This component is so broad that it extends beyond the photospheric Na I line at 10 837.814 Å on
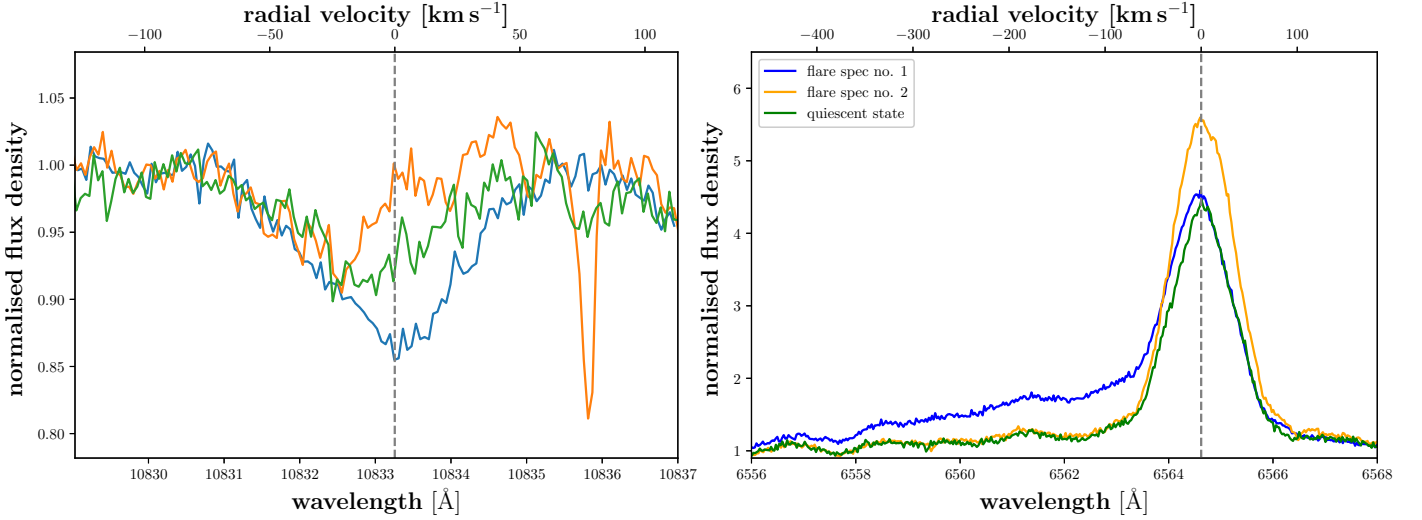
**Fig. 6.** Three of 14 spectra for different chromospheric indicator lines for RBS 365. *Left*: He I IR line. *Right*: Hα line. The spectrum with the pronounced blue wing in Hα corresponds to the deepest spectrum in He I IR (both indicated by the blue solid line corresponding to flare spectrum no. 1). The green spectra represent the most quiescent case and the orange line a more active state (flare spectrum no. 2), which may or may not be associated with flaring. The dashed vertical lines denote the central wavelength of the displayed chromospheric lines.
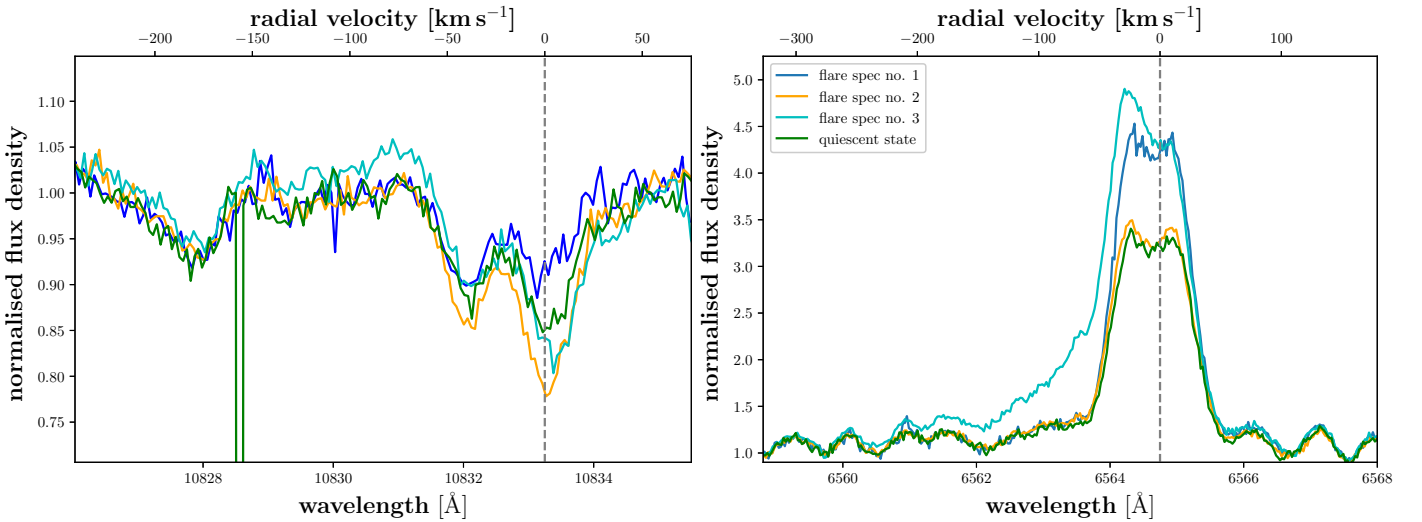


**Fig. 7.** Four out of six available spectra for different chromospheric indicator lines for J07472+503. *Left*: He I IR line. *Right*: Hα line. The dashed vertical lines indicate the central wavelength of the displayed chromospheric lines. The same colours indicate spectra corresponding to the same observation date; the corresponding dates are given in Table 4. The emission wing of the blue spectrum is most clearly seen at around 10 831 Å. The green spectrum represents the most inactive state.

the red side. The width of the line may be caused by turbulent broadening, but we deem it more probable that we are seeing material with a range of velocities blending into one broad line since the line extends on the red side to velocities of about 250-300 km s$^{-1}$ for both the He I IR line and Hα line. In this picture, the down-raining material produces Hα emission, while it is seen in absorption in the He I IR line. This suggests intermediate densities in the moving material, which are too low to drive the He I IR line into emission by collisions but sufficient to produce absorption. Red wings can be identified neither in the He I D$_3$ nor in the Ca II IRT lines.

The blue-shifted emission component in the He I IR line is also found in the He I D$_3$ and in the Ca II IRT lines. The velocity shift is about −7 km s$^{-1}$ for each of these lines. In the Hα line, this blue-shifted component is much less pronounced, producing only a slight enhancement of the blue line flank. We speculate

that this emission component originates from the flaring site and its velocity shift corresponds to the rotational velocity of the flaring region.

### 4.4. Symmetric line broadening of Hα

We found a number of examples for symmetric Hα line broadening, and all of these go along with He I IR line emission. In Fig. 9, we show six spectra of EV Lac, displaying cases that we consider symmetric Hα line broadening. The spectrum with the largest Hα enhancement by far (spectrum no. 2) also shows He I IR and He I D$_3$ line emission with broad wings. Apart from spectrum no. 6, the other spectra also display approximately symmetric broadening. Nevertheless, the symmetry is not perfect as, for example in spectra nos. 1 and 3. It remains unclear whether this is attributable to physical line asymmetries. We
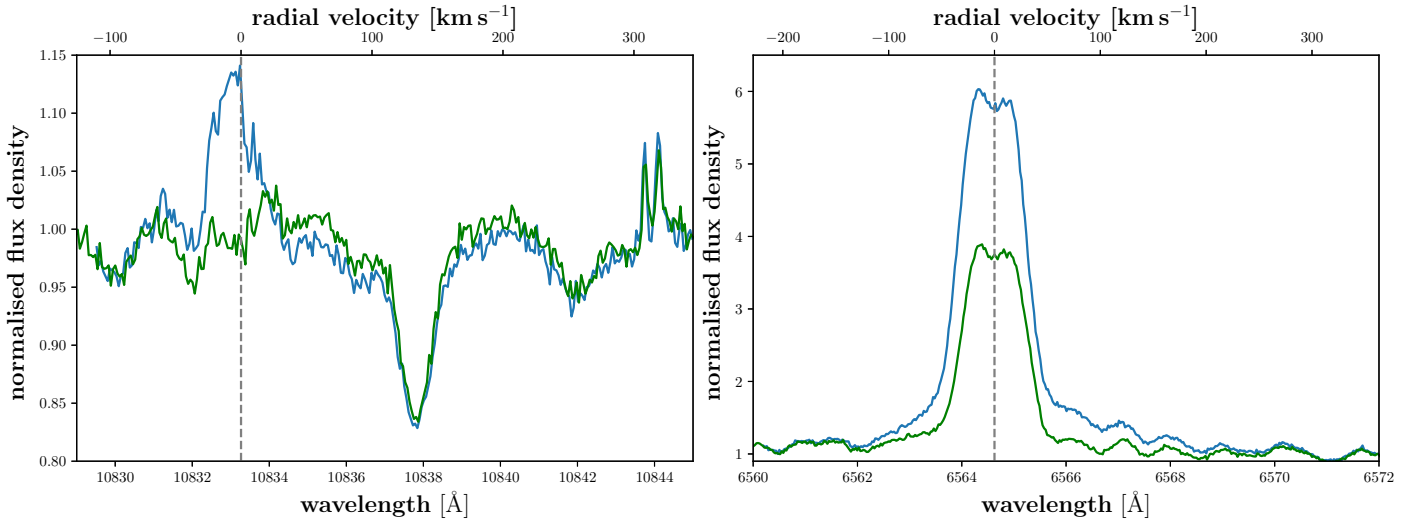
**Fig. 8.** Two of 11 spectra of GT Peg. *Left*: He I IR line. *Right*: Hα line. The green spectrum demonstrates the quiescent spectrum of the star.
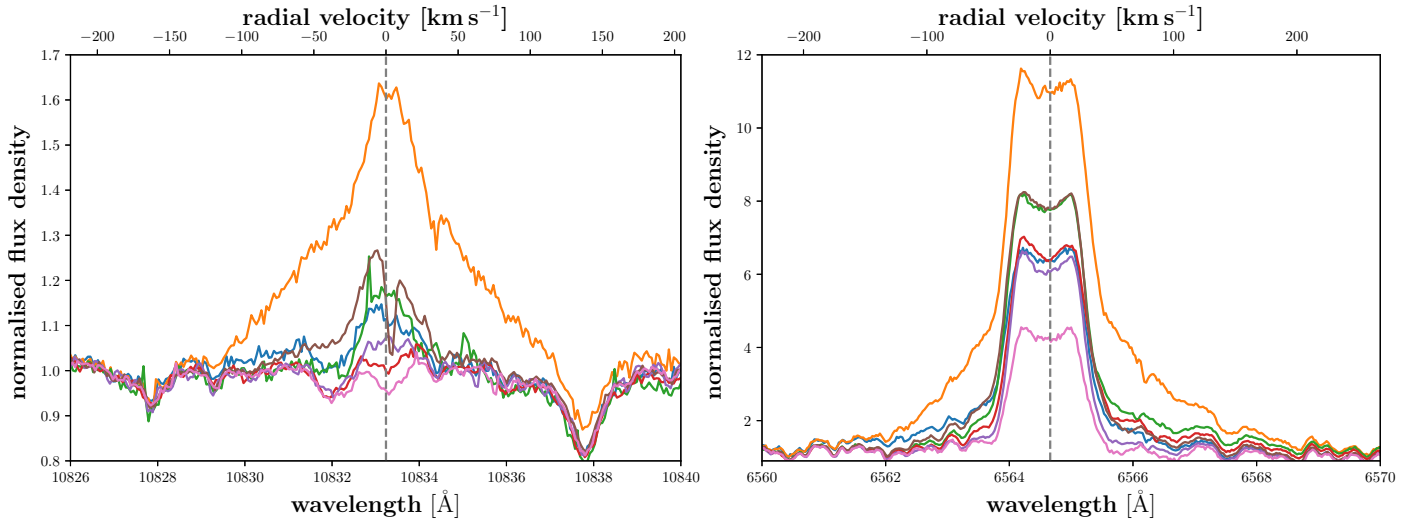


**Fig. 9.** Example spectra of the flaring activity state of EV Lac. *Left*: He I IR line going from nearly continuum level into clear emission. *Right*: Hα line. For both panels the colours correspond to the same observation times as described in Table 4. The pink spectrum represents the quiescent state of EV Lac.

speculate that at least some of these line profiles are caused by integration effects.

Another example, for which we identified a case of highly symmetric line broadening during a flare, is the star J11474+667 (1RXS J114728.8+664405) as can be seen in Fig. 10. This star shows no detectable He I IR IR line during the quiescent state, but displays large symmetric wings in the Hα, He I D₃, and He I IR lines during a large flare. Curiously, nothing similar is seen in the Ca II IRT lines. The Hα line wings extend to about ±400−450 km s⁻¹. The He I IR line wings span the ±100 km s⁻¹ range and that of the He I D₃ line still reaches ±50−70 km s⁻¹. The highest velocity material only seems to be bright in Hα, which may be attributable to low densities or a temperature favouring Hα emission. This may also be caused at least partially by the Stark effect, which affects the Balmer lines most strongly and is consistent with the non-detection of any wings in the Ca II IRT lines, which should not be affected by Stark broadening. Stark broadening could also explain the extreme width of the line since material at such high velocities is rarely observed

and the velocities are too high to be caused by Alfénic turbulence (Matthews et al. 2015; Lacatus et al. 2017), which typically causes line widths of the order of 100 km s⁻¹. The He I IR line normalised amplitude of this flare is among the largest of the whole sample.

### 4.5. LP 205-044

As one of the most outstanding examples of red and blue asymmetries, we show in Fig. 11 the spectra of the M5.0 star LP 205-044. Most of the spectra exhibit only moderate variation in the Hα line, which may be attributed to a quasi-quiescent state. However, two spectra with extreme Hα wings stand out. In both cases, the core of the Hα line reacts only weakly.

The spectrum no. 2 shows an extreme blue wing in the Hα line. A similar component can be distinguished in the He I IR line and, to a lesser extent, in the He I D₃ line. The mean shift of this component is about −120 km s⁻¹. The He I D₃ and the Ca II IRT lines simultaneously show a pronounced emission component
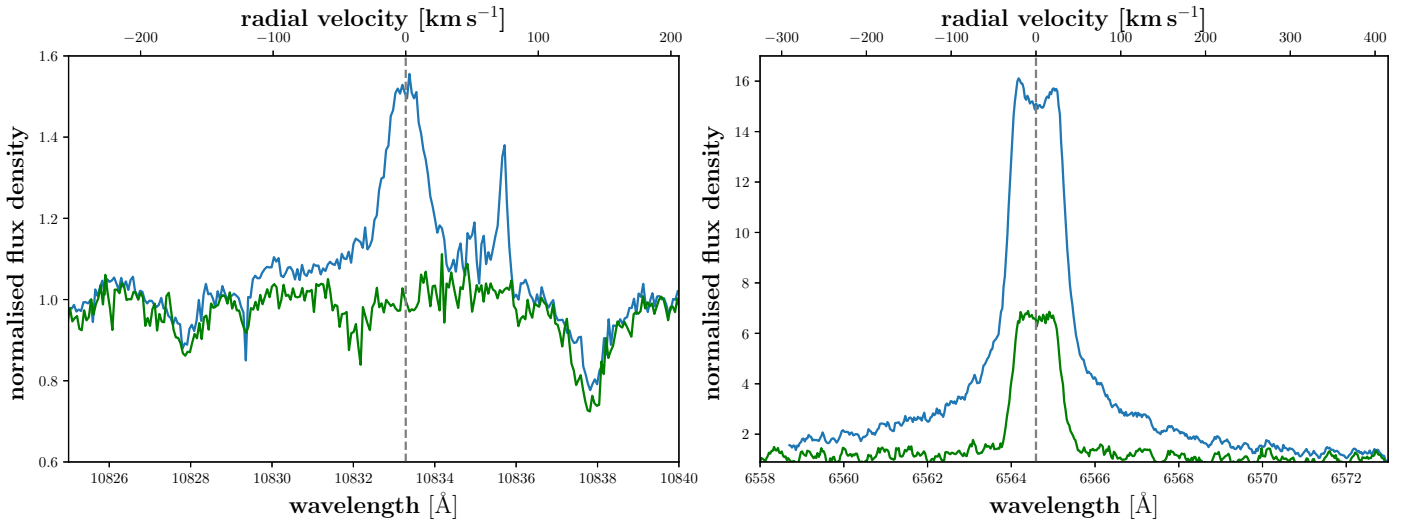
**Fig. 10.** Two of 21 available spectra for different chromospheric indicator lines for J11474+667. *Left*: He I IR line. *Right*: Hα line. The green spectrum illustrates the quiescent state.
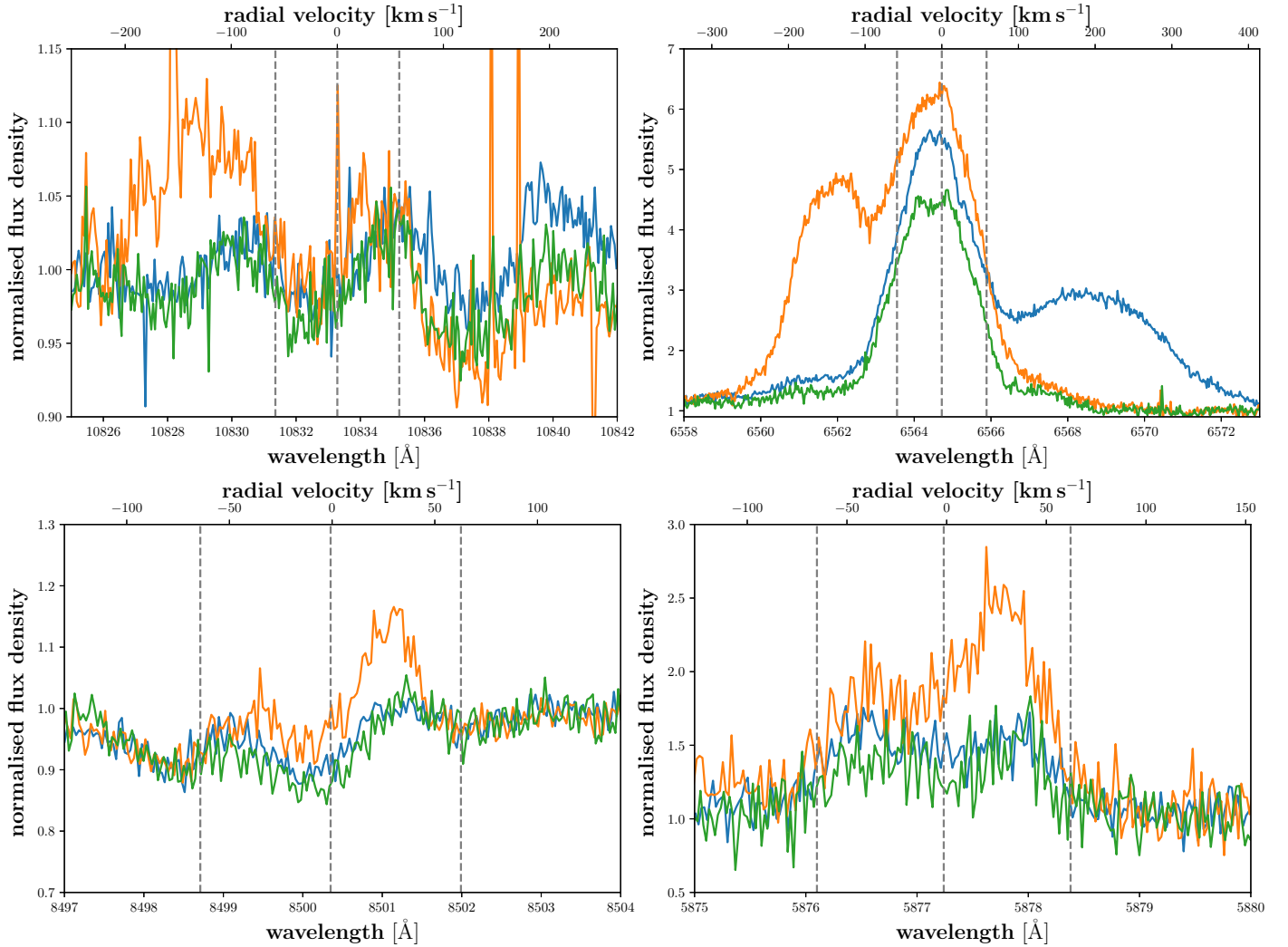


**Fig. 11.** Three of 22 available spectra for different chromospheric indicator lines for LP 205-044. *Top left*: He I IR line. *Top right*: Hα line. *Bottom left*: He I D$_3$ line. *Bottom right*: bluest Ca II IRT line. The dashed vertical lines indicate the central wavelength of the respective chromospheric lines and the wavelengths corresponding to the maximum rotational velocity of $v \sin i = 58.4$ km s$^{-1}$. The quiescent activity level is represented by the green spectra. The blue spectrum no. 1 is taken at JD 7823.44 and the orange spectrum no. 2 is taken at JD 8057.63 d.
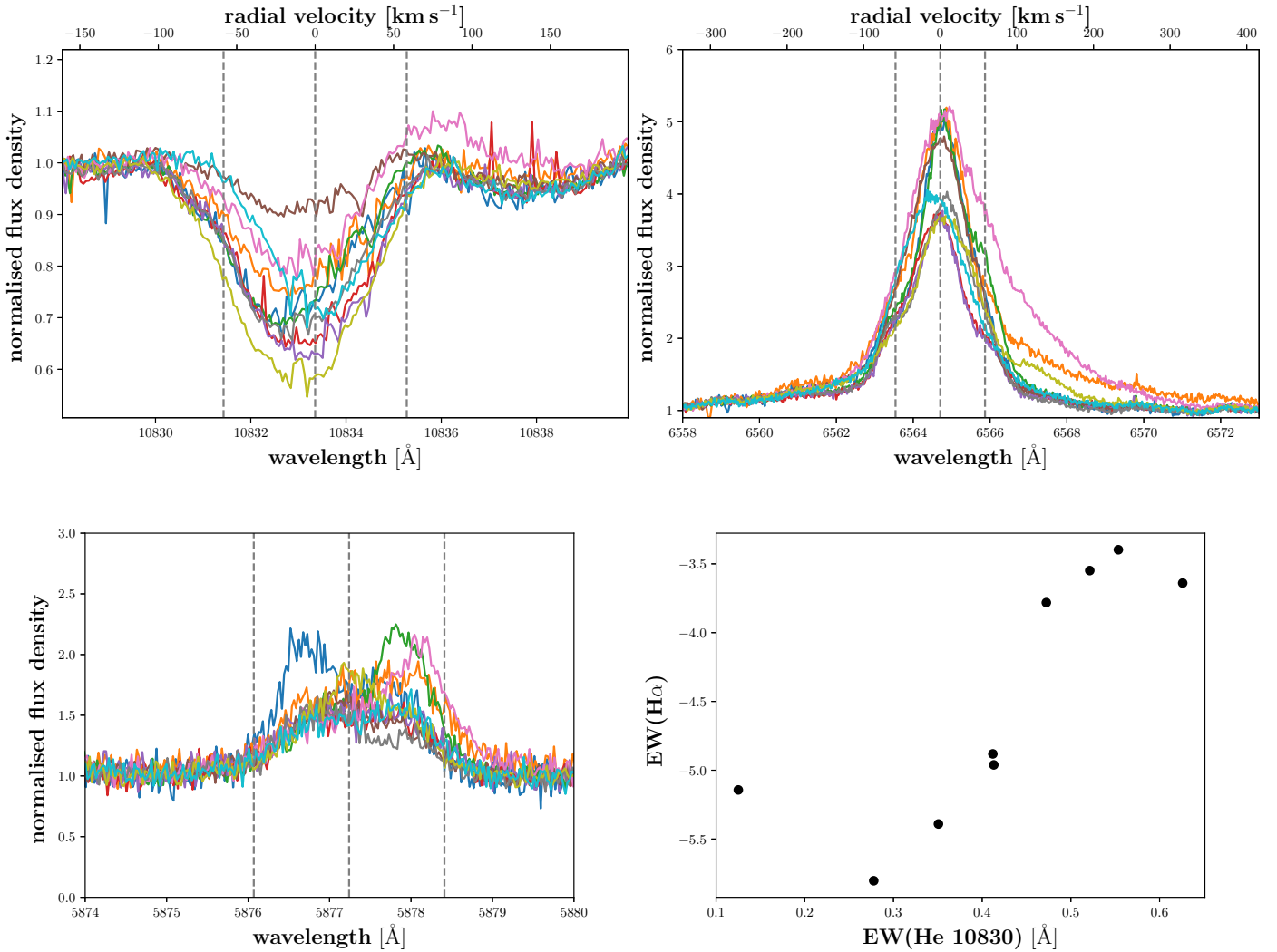
**Fig. 12.** Individual spectra for different chromospheric indicator lines for the M4.0 star Barta 161 12. *Top left*: He I IR line. *Top right*: Hα line. *Bottom left*: He I D$_3$ line. *Bottom right*: correlation between pEW(He I) and pEW(Hα).

red-shifted by about +30 km s$^{-1}$, that is within the rotational line profile. We speculate that this red-shifted component originates in the flare foot points, while the line wings trace evaporating material observed during the onset of a flare. The origin of a less strong blue-shifted component within the rotational profile of the He I D$_3$ and the Ca II IRT lines remains unclear.

In contrast, the spectrum no. 2 in Fig. 11 shows an enormous red Hα wing with a mean shift of about 180 km s$^{-1}$. The corresponding He I IR line spectrum shows a less prominent broad enhancement at a comparable shift. However, no such line enhancement is detectable in the He I D$_3$ or Ca II IRT lines. We hypothesise that this observation reflects coronal rain observed towards the end of a flare.

### 4.6. Barta 161 12

Barta 161 12 is a fast rotator with $v \sin i$ of 59.8 km s$^{-1}$ (Reiners et al. 2018) and a photometrically derived rotation period of 0.7 d (Kiraga 2012). As a candidate member of the β Pic moving group, the star is young with an estimated age of 12–22 Myr (Malo et al. 2013). The strong line broadening in this star leads to ubiquitous blends. In particular, the He I IR line is blended with the neighbouring, unidentified lines.

In Fig. 12, we show all ten He I IR, Hα, and He I D$_3$ spectra of Barta 161 12. The He I IR line especially shows an overall degree of variability, which is unmatched by any other target in our sample. By inspection of the He I D$_3$ line spectra, we identify four spectra with clear emission components (orange, magenta, green, and blue), which we attribute to flaring. However, also for the remaining spectra, no clear quiescent state can be identified in this star. This suggests that flaring is not the sole source of modulation of the chromospheric line profiles in Barta 161 12. Comparison of the pEWs of the Hα and He I IR lines shows a good correlation with elevated Hα emission being associated with fill-in of the He I IR line. A potential source of the observed variability is rotational modulation. To test this hypothesis, however, short-cadence spectroscopy, sampling the rotation period would be required. Its high level of overall variability makes Barta 161 12 a highly promising target for short-cadence follow-up.

## 5. Implications for exoplanet atmosphere studies

For more than half of the stars with He I line variability, the line pEW is also correlated to pEW(Hα). Low correlation coefficients for these stars are normally caused by outliers owing to

telluric artefacts, noise, or flaring activity. On the other hand, for non-variable stars the pEW(He I) is indeed constant even if some variation in pEW(H$\alpha$) or pEW(Ca II IRT$_1$) is present. This implies a comparable insensitivity of the stellar He I IR line to activity phenomena on M dwarfs, which is a favourable property for planetary atmospheric studies, for example by He I IR line transmission spectroscopy. The generally good relation between the pEW changes observed in the He I IR line with other activity indicators furthermore allows us to identify He I IR line variability by monitoring more sensitive chromospheric lines, such as the H$\alpha$ or Ca II H & K lines, if available in the spectrum, which we strongly recommend.

While choosing inactive host stars is an obvious route to minimise activity-related inference in planetary atmospheric studies, the peculiar formation of the He I IR line makes higher host star activity levels desirable for studies of planetary He I IR lines (e.g. Nortmann et al. 2018; Salz et al. 2018). Fortunately, our study suggests that variations in the stellar He I IR line remains comparably insensitive and a non-variable H$\alpha$ line also implies a stable He I IR line. The relation may break down in strong flares, which are however recognised with little difficulty in virtually all chromospheric lines.

For searches of the He I IR line in planetary atmospheres our outstanding examples are also instructive. The snapshot character of our data prevents us from estimating timescales on which the stellar He I IR line is variable and from comparing these variability timescales to timescales of in-transit phases of exoplanets. Nevertheless, the possibly strong reaction of the stellar He I IR line to especially larger flares shows that timescales of variation can be in the range of minutes, again showing the need to monitor the stellar chromospheric variability using other chromospheric lines.

Moreover, we studied the more than 100 spectra of EV Lac, of which many are taken only a day apart. This active M3.5 dwarf reveals a very shallow line at best by visual inspection. Also, the He I IR line seems to be stable for much of the time, with episodes of increased activity and a number of flares causing the variability.

## 6. Conclusions

We present a variability study of the He I IR line as observed in 319 M dwarfs by inspecting more than 14 000 CARMENES spectra. We find that the He I IR line can be very stable especially for early M dwarfs with H$\alpha$ in absorption. Nevertheless, we find variability in 56 (18%) out of 319 stars in this line. All of these stars show H$\alpha$ in emission, and if we examine only the subsample of stars with $v \sin i > 25$ km s$^{-1}$ we find about 80 percent of these stars to be variable in the He I IR line. Also mid-type M dwarfs, which were found in our previous paper (Fuhrmeister et al. 2019a) to display no He I IR line in the average spectrum, exhibit some He I line variability. For many of these stars the He I line occasionally turns from an absorption into an emission line, thus averaging out in the mean spectrum; this is, for example, the case for G 080-021 in Fig. 3. Alternatively, the star does not display a He I line during the quiescent state, but does so during the flaring state, as shown, for example, by J22518+317/GT Peg in Fig. 8. Most stars that are variable in the He I line are mid-type M3.0 to M6.0 V stars, where a steep decline for the line detection or no line detection at all is found for the average spectrum.

Generally, the He I IR line correlates well with H$\alpha$ if it shows detectable variability. For stars whose He I IR line shows no variability, H$\alpha$ may nevertheless do so, leading to non-correlation in these cases and stressing the relative insensitivity of the He I IR line to intrinsic variability; this makes the line a promising target for atmospheric studies of exoplanets using transmission spectroscopy.

Moreover, we present a number of outstanding examples of chromospheric line variations attributable to flares. Flaring activity manifests itself in H$\alpha$ line broadening combined with possible line asymmetries. A deepening of the He I IR line is typically observed during flare onset, where the H$\alpha$ line is still only marginally enhanced and often exhibits blue asymmetries as caused by chromospheric evaporations, which are thought to characterise the early stages of flare evolution. The deepening is likely produced by enhanced EUV and X-ray irradiation levels of the stellar atmosphere caused by the flare and therefore larger photon-ionisation and recombination rates of He I. In later flare stages, the He I IR line tends to go into emission. All H$\alpha$ spectra exhibiting symmetric broadening or red asymmetries also have He I IR emission lines, regardless of whether the line is observed in absorption or remains undetectable during the quiescent state of the star. Different chromospheric lines may behave similarly in terms of velocity shift, but there can also be remarkable differences, which we cannot currently explain. This may be caused by the snapshot character of our observations. Clearly, a detailed analysis of the He I IR line variability on shorter flare and transit timescales would greatly benefit from continuous, short-cadence time series observations.

## References

Allart, R., Bourrier, V., Lovis, C., et al. 2018, Science, 362, 1384
Alonso-Floriano, F. J., Morales, J. C., Caballero, J. A., et al. 2015, A&A, 577, A128
Alonso-Floriano, F. J., Snellen, I. A. G., Czesla, S., et al. 2019, A&A, 629, A110
Andreasen, D. T., Sousa, S. G., Delgado Mena, E., et al. 2016, A&A, 585, A143
Andretta, V., Giampapa, M. S., Covino, E., Reiners, A., & Beeck, B. 2017, ApJ, 839, 97
Baliunas, S. L., Donahue, R. A., Soon, W. H., et al. 1995, ApJ, 438, 269
Barnes, J. R., Jeffers, S. V., Haswell, C. A., et al. 2017, MNRAS, 471, 811
Berdyugina, S. V., & Järvinen, S. P. 2005, Astron. Nachr., 326, 283
Cauley, P. W., Kuckein, C., Redfield, S., et al. 2018, AJ, 156, 189
Cram, L. E., & Mullan, D. J. 1979, ApJ, 234, 579
Czesla, S., Molle, T., & Schmitt, J. H. M. M. 2018, A&A, 609, A39
Czesla, S., Schröter, S., Schneider, C. P., et al. 2019, PyA: Python astronomy-related packages
Díez Alonso, E., Caballero, J. A., Montes, D., et al. 2019, A&A, 621, A126
Doyle, L., Ramsay, G., Doyle, J. G., Wu, K., & Scullion, E. 2018, MNRAS, 480, 2153
Dupree, A., Brickhouse, N., Irwin, J., Kurucz, R., & Newton, E. 2018, in Cambridge Workshop on Cool Stars, Stellar Systems, and the Sun (Cambridge: Cambridge University Press), 87
Fouqué, P., Moutou, C., Malo, L., et al. 2018, MNRAS, 475, 1960
Fuhrmeister, B., Liefke, C., Schmitt, J. H. M. M., & Reiners, A. 2008, A&A, 487, 293
Fuhrmeister, B., Czesla, S., Schmitt, J. H. M. M., et al. 2018, A&A, 615, A14

Fuhrmeister, B., Czesla, S., Hildebrandt, L., et al. 2019a, A&A, 632, A24
Fuhrmeister, B., Czesla, S., Schmitt, J. H. M. M., et al. 2019b, A&A, 623, A24
Gizis, J. E., Monet, D. G., Reid, I. N., et al. 2000, AJ, 120, 1085
Hampel, F. R. 1974, J. Am. Stat. Assoc., 69, 383
Hawley, S. L., & Pettersen, B. R. 1991, ApJ, 378, 725
Hawley, S. L., Davenport, J. R. A., Kowalski, A. F., et al. 2014, ApJ, 797, 121
Hilton, E. J., West, A. A., Hawley, S. L., & Kowalski, A. F. 2010, AJ, 140, 1402
Hossain, M. M., Vineeth, C. N., Sumod, S. N. G. K., & Pant, T. K. 2014, Earth, Planets, and Space, 66, 56
Houdebine, E. R. 2012, MNRAS, 421, 3189
Jeffers, S. V., Schöfer, P., Lamert, A., et al. 2018, A&A, 614, A76
Kiraga, M. 2012, Acta Astron., 62, 67
Kowalski, A. F., Allred, J. C., Uitenbroek, H., et al. 2017, ApJ, 837, 125
Lacatus, D. A., Judge, P. G., & Donea, A. 2017, ApJ, 842, 15
Lépine, S., Hilton, E. J., Mann, A. W., et al. 2013, AJ, 145, 102
Malo, L., Doyon, R., Lafrenière, D., et al. 2013, ApJ, 762, 88
Malo, L., Artigau, É., Doyon, R., et al. 2014, ApJ, 788, 81
Mansfield, M., Bean, J. L., Oklopčić, A., et al. 2018, ApJ, 868, L34
Marfil, E., Tabernero, H. M., Montes, D., et al. 2020, MNRAS, 492, 5470
Martin, J., Fuhrmeister, B., Mittag, M., et al. 2017, A&A, 605, A113
Matthews, S. A., Harra, L. K., Zharkov, S., & Green, L. M. 2015, ApJ, 812, 35
Meunier, N., & Delfosse, X. 2009, A&A, 501, 1103
Mittag, M., Hempelmann, A., Schmitt, J. H. M. M., et al. 2017, A&A, 607, A87
Nagel, E., Czesla, S., Schmitt, J. H. M. M., et al. 2019, A&A, 622, A153
Newton, E. R., Irwin, J., Charbonneau, D., et al. 2016, ApJ, 821, 93
Newton, E. R., Irwin, J., Charbonneau, D., et al. 2017, ApJ, 834, 85
Nortmann, L., Pallé, E., Salz, M., et al. 2018, Science, 362, 1388
Oliva, E., Origlia, L., Scuderi, S., et al. 2015, A&A, 581, A47
Phillips, F., Burns, R., French, J. R., et al. 2004, Ann. Geophys., 22, 3315
Pizzolato, N., Maggio, A., Micela, G., Sciortino, S., & Ventura, P. 2003, A&A, 397, 147
Quirrenbach, A., Amado, P. J., Caballero, J. A., et al. 2016, Proc. SPIE, 9908, 990812
Rebull, L. M., Stauffer, J. R., Bouvier, J., et al. 2016, AJ, 152, 113
Reid, I. N., Hawley, S. L., & Gizis, J. E. 1995, AJ, 110, 1838
Reiners, A., Zechmeister, M., Caballero, J. A., et al. 2018, A&A, 612, A49
Riaz, B., Gizis, J. E., & Harvin, J. 2006, AJ, 132, 866
Robrade, J., & Schmitt, J. H. M. M. 2005, A&A, 435, 1073
Rousseeuw, P. J., & Croux, C. 1993, J. Am. Stat. Assoc., 88, 1273
Salz, M., Czesla, S., Schneider, P. C., et al. 2018, A&A, 620, A97
Sanz-Forcada, J., & Dupree, A. K. 2008, A&A, 488, 715
Schmidt, S. J., Kowalski, A. F., Hawley, S. L., et al. 2012, ApJ, 745, 14
Schöfer, P., Jeffers, S. V., Reiners, A., et al. 2019, A&A, 623, A44
Seager, S., & Sasselov, D. D. 2000, ApJ, 537, 916
Shkolnik, E., Liu, M. C., & Reid, I. N. 2009, ApJ, 699, 649
Shulyak, D., Reiners, A., Nagel, E., et al. 2019, A&A, 626, A86
Spake, J. J., Sing, D. K., Evans, T. M., et al. 2018, Nature, 557, 68
Suárez Mascareño, A., Rebolo, R., & González Hernández, J. I. 2016, A&A, 595, A12
Suárez Mascareño, A., Rebolo, R., González H ernández, J. I., et al. 2018, A&A, 612, A89
Tal-Or, L., Zechmeister, M., Reiners, A., et al. 2018, A&A, 614, A122
Vaughan, Jr., A. H., & Zirin, H. 1968, ApJ, 152, 123
Walkowicz, L. M., & Hawley, S. L. 2009, AJ, 137, 3297
Walkowicz, L. M., Basri, G., Batalha, N., et al. 2011, AJ, 141, 50
Wright, J. T., Marcy, G. W., Butler, R. P., & Vogt, S. S. 2004, ApJS, 152, 261
Yang, H., Liu, J., Gao, Q., et al. 2017, ApJ, 849, 36
Zechmeister, M., & Kürster, M. 2009, A&A, 496, 577
Zechmeister, M., Anglada-Escudé, G., & Reiners, A. 2014, A&A, 561, A59
Zirin, H. 1982, ApJ, 260, 655
Zirin, H. 1988, Astrophysics of the Sun (Cambridge: Cambridge University Press)